ELSEVIER

Ceramics International 33 (2007) 931–936

CERAMICS INTERNATIONAL

www.elsevier.com/locate/ceramint

Synthesis of tungsten oxide nanoparticles by acid precipitation method

Sitthisuntorn Supothina [a,*], Panpailin Seeharaj [b], Sorachon Yoriya [a], Mana Sriyudthsak [c]

[a] *National Metal and Materials Technology Center, 114 Thailand Science Park Paholyothin Rd., Klong Luang, Pathumthani 12120, Thailand*

[b] *Department of Materials Science, Faculty of Graduate College, King Mongkut's Institute of Technology North Bangkok, Pibulsongkram Rd., Bang Sue, Bangkok 10800, Thailand*

[c] *Department of Electrical Engineering, Faculty of Engineering, Chulalongkorn University, Phyathai Rd., Patumwan, Bangkok 10330, Thailand*

Received 21 November 2005; received in revised form 21 January 2006; accepted 14 February 2006
Available online 18 April 2006

Abstract

Tungsten oxide (WO_3) nanoparticle having average size of 30 nm, and nanoplate having average dimension of 190 ± 15 nm wide and 50 ± 5 nm thick were prepared by controlling a precipitation of ammonium tungstate para pentahydrate with nitric acid. The two nanostructured microstructures were obtained by varying the stirring time during the precipitation reaction while the other synthesis parameters were identical. Phase transition of the WO_3 precipitate was investigated by means of thermal analysis and X-ray diffraction, while the microstructure was observed by using a scanning electron microscope and a transmission electron microscope. The effect of the concentrations of the tungstate salt and nitric acid on the rate of precipitation and the percent yield of the precipitating product is also described.

Keywords: Tungsten oxide; Nanoparticle; Nanoplate; Precipitation

1. Introduction

Tungsten oxide (WO_3) is an n-type semiconductor with a reported band gap of about 2.6–2.8 eV [1]. The intrinsic conductivity arises from its non-stoichiometric composition giving rise to a donor level formed by oxygen vacancy defect in the lattice. Since the tungsten has many oxidation states, i.e., 2, 3, 4, 5 and 6, the tungsten compound can exist in many forms. For instance, the typical forms of tungsten oxides are tungsten (VI) oxide (WO_3, lemon yellow appearance) and tungsten (IV) oxide (WO_2, brown and blue appearance) [2]. Such electronic properties make the tungsten oxides suitable for various applications such as electrochromic [3], photochromic [4], photocatalyst [5], and gas sensor [6–8]. The WO_3 nanoparticles or nanocrystallites have been synthesized by various techniques such as pyrolysis [5,6], thermal decomposition [9], and wet chemical processes such as sol–gel [10], colloidal process [4], and ion-exchange method [11,12].

For wet chemical processes, the tungsten (hydrous) oxides either in the form of sol, gel or particles, were typically prepared via hydrolysis of the tungstate salts in acidic medium, either by direct mixing of the salts and the acid, or by passing the tungstate salt solution through an ion-exchange resin. For instance, Sun et al. [4] precipitated the tungsten trioxide dihydrate ($WO_3{\cdot}2H_2O$) gel by dropwise addition of a concentrated hydrochloric acid (HCl) in a solution of sodium tungstate dihydrate ($Na_2WO_4{\cdot}2H_2O$). Then, the $WO_3{\cdot}2H_2O$ colloids were formed at lower pH by dissolving the gel in a concentrated oxalic acid solution. By using an appropriate concentration of the oxalic acid, the nanometer-size (10–30 nm) tungsten oxide particles were obtained. Similarly Balazsi and Pfeifer [13] obtained an amorphous gel of $WO_3{\cdot}2H_2O$ by mixing a $Na_2WO_4{\cdot}2H_2O$ solution with 1N HCl solution at 5 °C. The amorphous gel was found to crystallize upon washing with water. In a different approach, Choi et al. [11] prepared the $WO_3{\cdot}2H_2O$ sols (~30 nm) by flowing a Na_2WO_4 solution through a column packed with protonated cation-exchange resin. Post treatment of these sols by centrifuging resulted to the tungsten oxide crystallites having preferred orientation.

* Corresponding author. Tel.: +66 2 564 6500; fax: +66 2 564 6447.
E-mail address: sitthis@mtec.or.th (S. Supothina).

0272-8842/$32.00
doi:10.1016/j.ceramint.2006.02.007

In this study, we synthesized the WO_3 nanoparticles by controlling the precipitation reaction of the ammonium tungstate solution and nitric acid solution by using dilute concentration of the tungsten salt. The WO_3 nanoplates were obtained by extending the stirring time during the precipitation reaction.

2. Experimental

2.1. Materials synthesis

The WO_3 nanostructures were synthesized by precipitation technique from aqueous solutions of ammonium tungstate para pentahydrate ($(NH_4)_{10}W_{12}O_{41}\cdot 5H_2O$, Wako) and nitric acid (HNO_3, Merck). A pre-determined amount of the tungstate salt was dissolved in de-ionized water and the resulting solution was brought to 80 °C. With vigorous stirring, a warm, concentrated nitric acid was added dropwise. The amounts of the tungstate salt and nitric acid were used such that the final concentrations of both reactants were in the range of 5.3–16.0 mM and 1.5–6.0 M, respectively, to study the effect of reactant concentrations on a precipitation rate and yield of the precipitating product. With continuous stirring, the mixed solution was kept at 80 °C for 30–60 min, after which the precipitates were allowed to settle for 1 day at room temperature. The precipitate was washed by addition of a large amount of de-ionized water into the precipitate followed by stirring for about 10 min and allowing the precipitates to settle down overnight before decanting the liquid. This washing procedure was carried out twice. Finally, the precipitates were separated by ultrafiltration using a polymer membrane (pore size = 0.47 μm). After drying at 100 °C overnight, the precipitates were calcined in air at temperatures ranging from 150 to 800 °C for 2 h. In some experiments, the as-precipitates were dried at room temperature under vacuum before subjected to crystal structure analysis.

2.2. Materials characterization

Phase evolution of the tungsten oxide nanostructures upon heat treatment was studied using thermogravimetric analysis (TGA; Perkin-Elmer TGA7), differential thermal analysis (DTA; Perkin-Elmer DTA7). Crystal structure was studied using an X-ray diffractometer (XRD; JEOL JDX-3503). Particle morphology was examined using a field-emission scanning electron microscope (FE-SEM; JEOL JSM-6301F) and a transmission electron microscope (TEM; JEOL JEM-2010). The crystallite size (D, in Å unit) was calculated from peak broadening using the Scherrer approximation, which is defined as

$$D = \frac{0.9\lambda}{B\cos\theta} \tag{1}$$

where λ is the wavelength of the X-ray (1.5418 Å), B is the full width at half maximum (FWHM, radian) and θ is the Bragg angle (degree). The value of FWHM was obtained by performing profile fitting using an XRD pattern processing software (Jade 6.5). The instrumental line broadening was corrected by using an NIST 640A silicon standard. The amount of possible ammonium residue in the precipitate was analyzed by measuring the nitrogen content using an X-ray fluorescence (XRF, Philips PW-2404) and an energy-dispersive X-ray spectrometer (EDS, Oxford INCA 300/6587) attached to the SEM unit. The specific surface area was measured by means of nitrogen adsorption using Quantachrome Autosorb-1 and then calculated by using a Brunauer, Emmett and Tellet (BET) method.

3. Results and discussion

3.1. Effect of precursor concentrations on the precipitation rate and yield

It was observed that a rate of precipitation was dependent on concentrations of both reactants. At higher concentration, the onset of precipitation was observed at a shorter time. For instance at the concentration of 16 mM [W salt] and 6 M [HNO_3], the precipitation took place within few seconds upon completion of acid addition, whereas at concentration of 5.3 mM [W salt] and 1.5 M [HNO_3], the precipitation was observed after about 10 min of aging.

The effect of reactant concentration on the rate of precipitation can be explained based on the activation energy (ΔG^*) required to form a critical nucleus of the solid of radius r^* which is defined by [14]:

$$\Delta G^* = \frac{16\pi\sigma^3 M^3}{3(\rho RT\ln S)^2} \tag{2}$$

where σ is the interfacial tension between the precipitate and its surroundings, ρ is the precipitate density, M is the molecular weight of the precipitate, and S is the supersaturation, which is defined by:

$$S = \frac{c}{c^*} \tag{3}$$

where c is the concentration of the hydrolyzed tungsten species such as $W_6O_{20}(OH)^{5-}$, $W_{12}O_{39}{}^{6-}$, $W_{12}O_{38}(OH)_2{}^{6-}$ or $W_{12}O_{41}{}^{10-}$, depending on the solution's pH and concentration [15], and c^* is the concentration of the solution in equilibrium with the precipitate at the reaction temperature. Eq. (2) indicates that the activation energy can be decreased (and, therefore, nucleation promoted) by increasing supersaturation of the solution. In this system, the degree of supersaturation increased with increasing concentrations of nitric acid (reducing pH) and the tungstate salt.

Fig. 1 shows a percent yield of the dried precipitates prepared at various concentrations of the tungstate salt and nitric acid. The reaction time was 30 min. The yield was calculated on the basis of the precipitating product of the two reactants, together with the results from thermal analysis and XRD which will be described later, as shown in Eq. (4).

$$(NH_4)_{10}W_{12}O_{41}\cdot 5H_2O + 10HNO_3 + 2H_2O = 12WO_3\cdot H_2O + 10NH_4{}^+ + 10NO_3{}^- \tag{4}$$

It is evident from Fig. 1 that, under the range of concentrations studied, the yield depended on the concentration of both

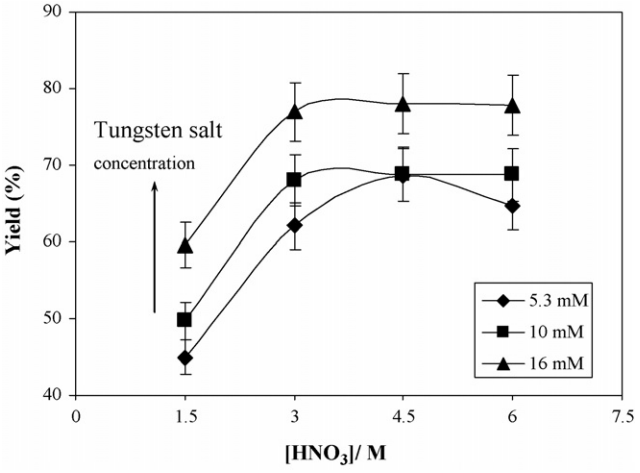

Fig. 1. Yield of the dried precipitates prepared at various concentrations of the ammonium tungstate para pentahydrate and nitric acid.

reactants. At any fixed concentration of nitric acid, the more concentrated solutions underwent faster precipitation and gave higher yield since the corresponding precursor solutions were more supersaturated. Extending the reaction time from 30 min to 1 h did not increase the yield indicating that the precipitation reaction was completed within 30 min. Similarly, at a certain tungstate salt concentration, the yield increased with increasing concentration of nitric acid and became constant at the acid concentration higher than 3 M. It was believed that at higher acid concentration, there was excess amount of acid that did not take part in the hydrolysis reaction shown in Eq. (4).

3.2. WO_3 nanoparticles

Fig. 2 shows a TGA and DTA results performed on the precipitate obtained by stirring the precursor solution for 30 min. According to the TGA result, slight weight loss was observed at ~40–120 °C due to an evaporation of physically adsorbed water. A major weight loss of 5.2% was observed at temperatures ranging from 150 to 300 °C with the maximum loss at ~220 °C. This weight loss was attributed to the loss of chemically bonded water of crystallization. The slight weight loss observed at temperatures between 300 and 400 °C may be attributed to some final water decomposition occurring during the crystallization of the amorphous phase. The total weight loss of 6.9% from the TGA data was close to the calculated weight loss of 7.2% based on the loss of H_2O from the $WO_3{\cdot}H_2O$ precipitate. The DTA result is in good agreement with the TGA data as two endothermic peaks were clearly observed at 100 and 260 °C due to the loss of physically adsorbed water and chemically bonded water, respectively.

Fig. 3 shows the XRD patterns of the precipitates dried under vacuum at room temperature (denoted as ''as-precipitate''), dried in an oven at 100 °C and calcined in air at temperatures ranging from 150 to 400 °C. By performing peak matching with the standard patterns, the as-precipitate, the dried precipitate and the precipitate calcined at 150 °C were identified as tungsten oxide monohydrate ($WO_3{\cdot}H_2O$), also known as tungstite, having orthorhombic structure (JCPDS# 43-0679)

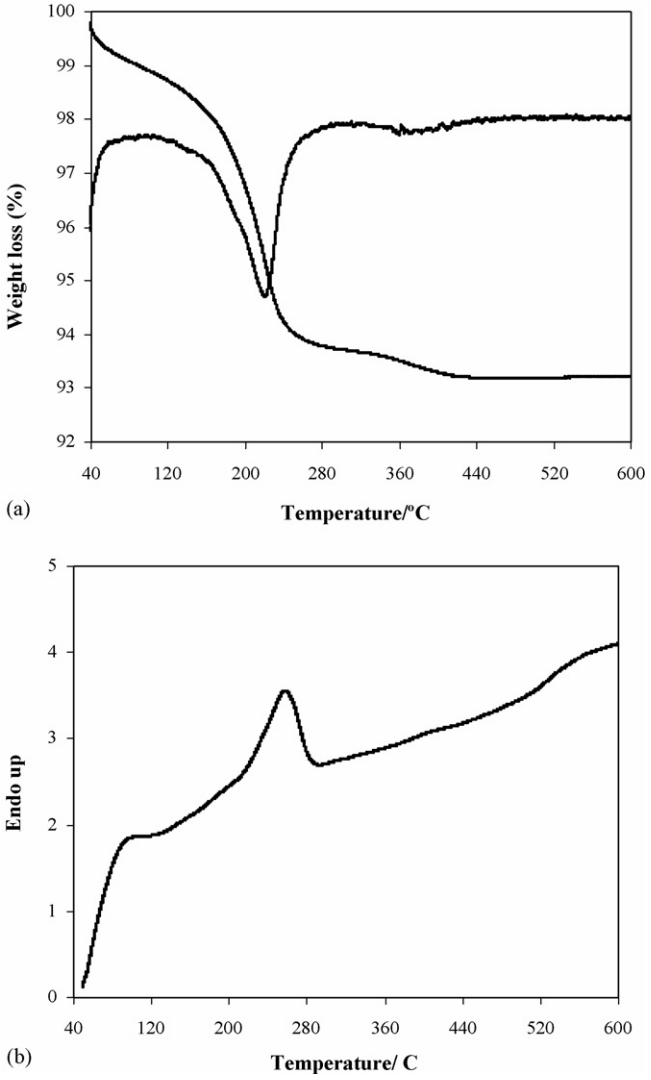

Fig. 2. (a) TGA and (b) DTA results of the dried tungsten oxide precipitate.

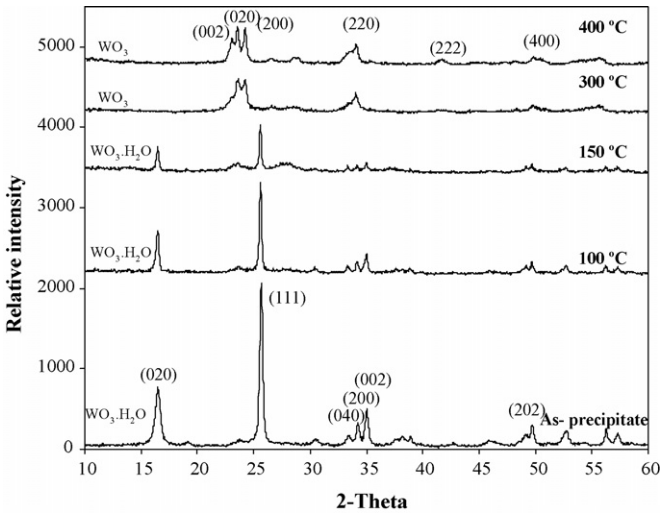

Fig. 3. XRD patterns of the as-precipitate, and the precipitates dried and calcined at various temperatures.

while the precipitates calcined at 300 °C and above were identified as WO_3 having monoclinic structure (JCPDS# 43-1035). The XRD results supported the results from thermal analysis that the $WO_3{\cdot}H_2O$ transformed to the WO_3 at around 220 °C. Note that the dried precipitates obtained from various solution concentrations had the same crystal structure. The more separated and sharper peaks and higher number of reflections were observed in the XRD patterns of the WO_3 calcined at higher temperatures, indicating an increase degree of crystallinity upon increasing calcination temperature.

The precipitating products formed by this current method (i.e., a yellow $WO_3{\cdot}H_2O$ powder) were different from those reported in the literature (i.e., a white or yellow $WO_3{\cdot}2H_2O$ gel) [4,11,13]. In this study, the supersaturated solution underwent particle nucleation with no intermediate gellation stage, whereas the supersaturated effluent solution from the ion-exchange column was unstable and transform into an opaque soft gel. The gel finally turned into a mixture of a crystalline $WO_3{\cdot}2H_2O$ and amorphous phase. By direct mixing $Na_2WO_4{\cdot}2H_2O$ solution with concentrated HCl until the solution became mild acidic (pH ∼ 4), Sun et al. [4] obtained a white, gelatineous precipitate which was re-dissolved with concentrated solution of oxalic acid and formed a transparent colloidal solution of $WO_3{\cdot}2H_2O$ by subsequent dilution. This discrepancy could be resulted from the formation of different hydrolysis products by these methods as a result of different tungsten salt and the type of acid employed. However, phase transformation of the hydrous tungsten oxide prepared in this work was similar to that prepared by ion-exchange method. That is, the $WO_3{\cdot}H_2O$ phase was converted to the anhydrous WO_3 phase at ∼220–240 °C.

The crystallite size was then approximated from the XRD peaks using the Scherrer's formula (Eq. (1)) which relates the crystallite size to the peak broadening. The values of peak broadening were obtained by performing profile fitting of the major peaks, i.e., (0 0 2), (0 2 0) and (2 0 0) for the WO_3, and (1 1 1) and (0 2 0) for the $WO_3{\cdot}H_2O$. The peaks became narrower with increasing calcination temperature, based on Scherrer's approximation, indicating the increase of the crystallite size. The calculated crystallite size at various calcination temperatures is shown in Table 1. It was clear that the crystallite size increased upon heating to higher temperatures. However, the crystallite growth was not clearly observed at temperature <700 °C but became significant at temperature ≥700 °C. Extended heating time from 2 to 10 h also caused the crystallite growth but in less extent than the growth due to the temperature increase.

Calcination also had an effect on the specific surface area of the WO_3 particles. As summarized in Table 1, the specific surface area reduced from $9.5 \pm 0.5\ m^2\ g^{-1}$ for the particles calcined at 500 °C for 2 h to $1.6 \pm 0.1\ m^2\ g^{-1}$ for the particles calcined at 800 °C for the same period of time. In contrast, the specific surface area of the particles calcined at 500 °C for 2–10 h was almost unchanged. That is, it slightly reduced from $9.5 \pm 0.5\ m^2\ g^{-1}$ for 2-h calcination to $8.8 \pm 0.4\ m^2\ g^{-1}$ for 6-h calcination, and to $8.0 \pm 0.4\ m^2\ g^{-1}$ for 10-h calcination. It is obvious that calcination temperature had more profound effect than the calcination time. The reduction of surface area may be unfavourable in some applications, such as gas sensor in which a detection mechanism relies on gas adsorption/desorption on the oxide surface.

Table 1
The crystallite size and specific surface area of the tungsten oxide particles obtained at various calcination temperatures

Heat treatment condition		Crystallite size (nm, ±3 nm)	Specific surface area ($m^2\ g^{-1}$)
Temperature (°C)	Time (h)		
100	12	30	13.8 ± 0.7
400	6	27	10.6 ± 0.5
500	2	29	9.5 ± 0.5
	6	30	8.8 ± 0.4
	10	36	8.0 ± 0.4
600	2	–	6.0 ± 0.3
	6	31	5.5 ± 0.3
700	2	–	3.9 ± 0.2
	6	37	–
	10	–	3.4 ± 0.2
800	2	–	1.6 ± 0.1
	6	47	–
	10	–	2.1 ± 0.1

Fig. 4a shows an SEM image of the particles calcined in air at 400 °C for 6 h. Agglomerates with sizes ranging from 100 to

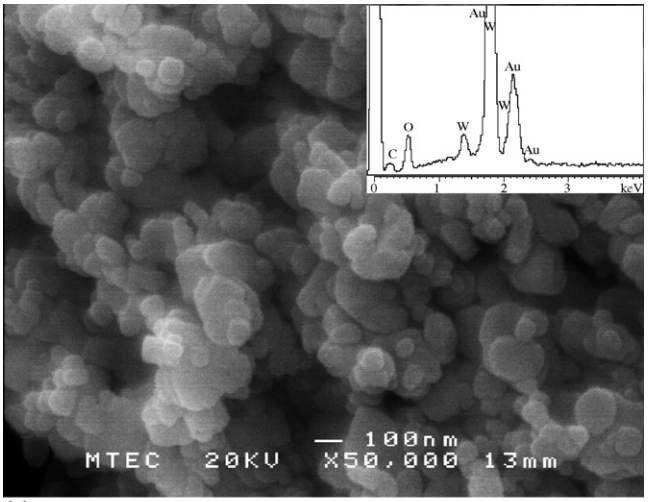

(a)

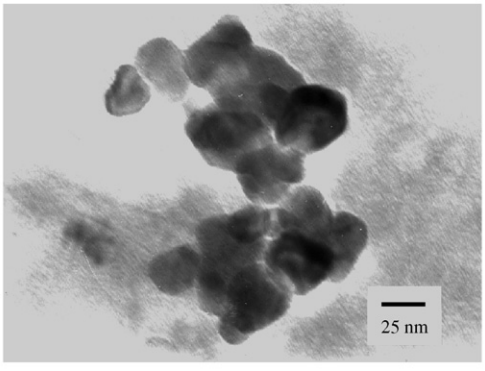

(b)

Fig. 4. (a) SEM images of the WO_3 particles calcined at 400 °C for 6 h. Inset is EDS spectrum; (b) TEM image of the same sample.

500 nm were distinctly observed. These agglomerates appeared to consist of finer primary particles which were too small to be clearly observed with the SEM employed. Higher magnification TEM image (Fig. 4b) revealed primary particles of average size ~30 nm. Some of these nanoparticles formed loose agglomeration of ~100 nm, corresponding to SEM observation. Note that the sizes of the particles observed by the TEM technique (30 nm) and by calculation from the XRD peaks (27 nm) were in the same range within an experimental error. Chemical analysis using EDS (inset, Fig. 4a) and XRF (not shown) techniques showed only W and O with no Cl and N residues.

3.3. WO_3 nanoplates

Fig. 5 shows SEM images of the dried precipitates obtained from the same precursor as the nanoparticle shown in Fig. 4, but the time of reaction was extended to 60 min. It is evident that under this treatment the nanoplate was obtained. The nanoplate has average dimension of 190 ± 15 nm wide and 50 ± 5 nm thick. Although the individual nanoplate has larger dimension than that of the primary nanoparticle, according to SEM observation the corresponding powder was less agglomerated and therefore was more porous. The specific surface area was 35.6 ± 1.8 $m^2\ g^{-1}$ which was almost three times higher than that of the nanoparticle obtained under identical precipitation condition but shorter stirring time, confirming the SEM observation that the nanoplate powder was more porous. Fig. 6 is an XRD pattern of the WO_3 nanoplate calcined in air at 500 °C for 2 h. By comparing the XRD patterns of the nanoparticle and nanoplate, the (0 0 2) reflection of the nanoplate was significantly attenuated suggesting that the sample had preferred orientation. Thermal analysis of the WO_3 nanoplate also gave similar results as those of the nanoparticle.

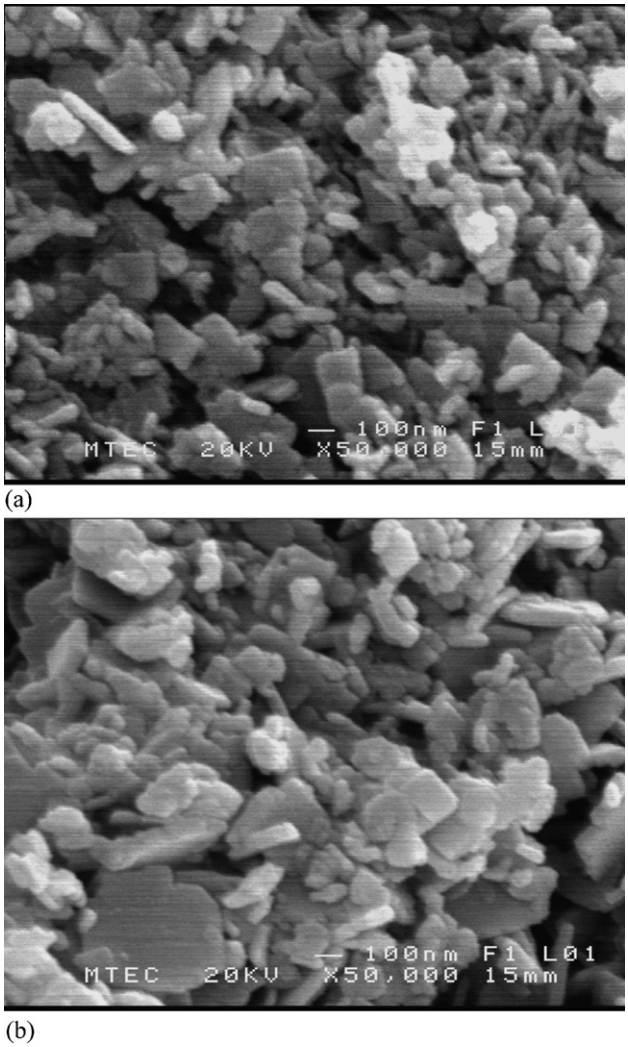

Fig. 5. SEM images of the WO_3 nanoplate prepared from the same condition for the preparation of the nanoparticles shown in Fig. 4 but the stirring time was extended to 1 h. (a) Dried nanoplate, and (b) nanoplate calcined at 400 °C for 2 h.

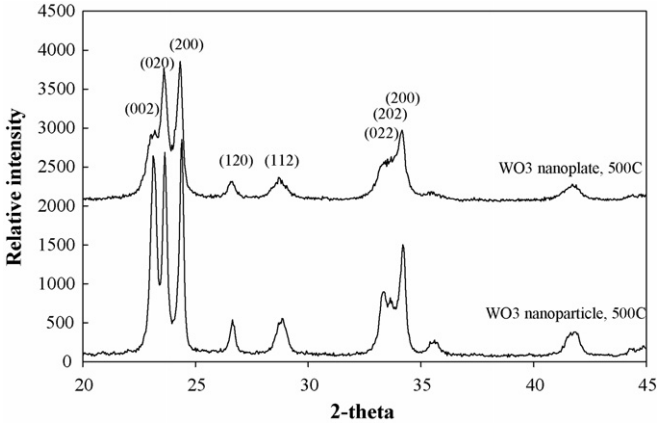

Fig. 6. XRD patterns of the nanoparticle and nanoplate prepared from the same solution but different stirring time, and then calcined at 500 °C.

4. Conclusions

The WO_3 nanoparticles were synthesized by precipitation reaction between the ammonium tungstate para pentahydrate and nitric acid. Extending the stirring time of the precursor solution had no effect on the percent yield of the precipitating product but led to the formation of the nanoplate. The yield of the precipitating product was found to increase with increasing degree of supersaturation of the solution which increased upon increasing concentrations of both reactants. Regardless of the particle morphology, the dried precipitates were orthorhombic $WO_3{\cdot}H_2O$, which transformed to the more stable monoclinic WO_3 at 220 °C.

Acknowledgements

This research was supported by the National Metal and Materials Technology Center, the National Science and Technology Development Agency, Thailand (Grant MT-B-46-CER-07-143-NI). Miss Seeharaj would like to acknowledge the financial support of the Thailand Graduate Institute of Science and Technology.

References

[1] M.A. Butler, Photoelectrolysis and physical properties of the semiconducting electrode WO_3, J. Appl. Phys. 48 (1977) 1914–1920.

[2] Solid state structure of tungsten trioxide. Available online at http://www.webelements.com.

[3] C.G. Granqvist, Electrochromic tungsten oxide films: review of progress 1993–1998, Solar Ener. Mater. Solar Cell 60 (2000) 201–262.

[4] M. Sun, N. Xu, Y.W. Cao, J.N. Yao, E.G. Wang, Nanocrystalline tungsten oxide thin film: preparation, microstructure, and photochromic behaviour, J. Mater. Res. 15 (2000) 927–933.

[5] G.R. Bamwenda, H. Arakawa, The visible light induced photocatalytic activity of tungsten trioxide powders, Appl. Catal. A 210 (2001) 181–191.

[6] M. Akiyama, J. Tamaki, N. Miura, N. Yamazoe, Tungsten oxide-based semiconductor sensor highly sensitive to NO and NO_2, Chem. Lett. (1991) 1611–1614.

[7] A.A. Tomchenko, V.V. Khatko, I. Emelianov, WO_3 thick-film gas sensor, Sens. Actuators B 46 (1998) 8–14.

[8] D.S. Lee, S.D. Han, J.S. Hun, D.D. Lee, Nitrogen oxide-sensing characteristic of WO_3-based nanocrystalline thick film gas sensor, Sens. Actuators B 60 (1999) 57–63.

[9] T. Inoue, K. Ohtsuka, Y. Yoshida, Y. Matsuura, Y. Kajiyama, Metal oxide semiconductor NO_2 sensor, Sens. Actuators B 24–25 (1995) 388–391.

[10] J.J. Shieh, H.M. Feng, M.H. Hon, H.Y. Juang, WO_3 and W-Ti-O thin film gas sensors prepared by sol-gel dip-coating, Sens. Actuators B 86 (2002) 75–80.

[11] Y.G. Choi, G. Sakai, K. Shimanoe, N. Miura, N. Yamazoe, Preparation of aqueous sols of tungsten oxide dehydrate from sodium tungstate by an ion-exchange method, Sens. Actuators B 87 (2002) 63–72.

[12] Z. Lu, S.M. Kanan, C.P. Tripp, Synthesis of high surface area monoclinic WO_3 particles using organic ligands and emulsion based methods, J. Mater. Chem. 12 (2002) 983–989.

[13] Cs. Balazsi, J. Pfeifer, Structure and morphology changes caused by wash treatment of tungstic acid precipitates, Solid State Ionics 124 (1999) 73–81.

[14] J.W. Mullin, Crystallization, Butterworth, UK, 1972.

[15] C.F. Baes, R.E. Mesmer, The hydrolysis of cations, John Wiley & Sons, New York, 1986.